



Universiteit
Leiden
The Netherlands

The innate immune response against mycobacterial infection : analysis by a combination of light and electron microscopy

Hosseini, R.

Citation

Hosseini, R. (2015, October 20). *The innate immune response against mycobacterial infection : analysis by a combination of light and electron microscopy*. Retrieved from <https://hdl.handle.net/1887/35954>

Version: Not Applicable (or Unknown)

License: [Licence agreement concerning inclusion of doctoral thesis in the Institutional Repository of the University of Leiden](#)

Downloaded from: <https://hdl.handle.net/1887/35954>

Note: To cite this publication please use the final published version (if applicable).

Cover Page



Universiteit Leiden



The handle <http://hdl.handle.net/1887/35954> holds various files of this Leiden University dissertation.

Author: Hosseini, Rohola

Title: The innate immune response against mycobacterial infection : analysis by a combination of light and electron microscopy

Issue Date: 2015-10-20

CHAPTER 4

ULTRASTRUCTURAL ANALYSIS OF THE EFFECT OF MYD88 DEFICIENCY ON GRANULOMA DEVELOPMENT DURING MYCOBACTERIUM MARINUM INFECTION

Rohola Hosseini, Gerda E. M. Lamers, Erik Bos, Abraham J. Koster,
Annemarie H. Meijer, Herman P. Spaink, Marcel J. M. Schaaf

Manuscript in preparation

Summary

Myeloid differentiation factor 88 (Myd88) is the key adapter protein of Toll-like receptors (TLRs), which initiate the innate immune response upon activation. Myd88 deficiency during bacterial infection affects innate immune responses including production of cytokines and reactive oxygen species (ROS) and initiation of autophagic defence. Using a *myd88* zebrafish mutant, we investigated the morphology of granulomas during the course of *Mycobacterium marinum* (*Mm*) infection in a tail fin infection model. Light microscopy images show that *Mm* granulomas formed in the tail fin of *myd88* mutants have different morphological features compared to the infection in the wild type, including a more compact structure, a reduced recruitment of leukocytes and a reduced number of TUNEL-positive dead cells. These morphological differences were associated with an increased bacterial burden in the *myd88* mutant. Ultrastructural electron microscopy analysis showed that the majority of *Mm* in the *myd88* mutant is extracellular. The intracellular bacteria in the *myd88* mutant were mainly present in phagosomal compartments or occur as aggregates, which were not acidic. In contrast, in the granulomas of wild type larvae 46% of *Mm* are found in intracellular acidic compartments, including acidic aggregates, lysosomes and autophagic compartments. In *myd88* mutants only 13% of *Mm* is present in such acidic compartments. These observations suggest that the Myd88-dependent recruitment of leukocytes is necessary for reuptake of dead infected cells and that subsequent acidification of large bacterial aggregates taken up from dead cells restricts bacterial growth in the infected tissue.

Introduction

Pulmonary tuberculosis (TB) is a bacterial infection caused by *Mycobacterium tuberculosis* (*Mtb*), which is estimated to have infected one third of the global population. Currently, over a million people do not survive this infection each year (WHO, 2014: http://www.who.int/tb/publications/global_report/en/). Increasing occurrence of multi-drug resistant *Mtb* strains is wide spread, and in order to develop novel therapeutic strategies a better understanding of the *Mtb* pathogenesis is required (Koul et al., 2011; Goldberg et al., 2012).

During the pathogenesis of TB, *Mtb* displays a complex interaction with the immune system of the host. *Mtb* is phagocytized by macrophages, where it prevents lysosomal degradation by inhibiting phagosome-lysosome fusion (Armstrong and Hart 1971; Russel, 2007). In addition, there is evidence that *Mtb* is able to escape from the phagosomes into the cytoplasm (van der Wel et al., 2007; Simeone et al., 2015). In these infected cells the *Mtb* bacteria create a niche, in which they can survive and replicate (Vergne et al., 2004; Russel et al., 2010).

Pro-inflammatory signals from infected macrophages initiate the recruitment of other innate and adaptive immune cells to the primary infection site, leading to the formation of highly organized granulomatous lesions. In these granulomas *Mtb* can persist for many years, forming a latent infection by minimizing its metabolic and replicative activity. However, *Mtb* can be reactivated resulting in an active TB infection (Gengenbacher et al., 2012).

Despite that *Mtb* exploits, macrophages to persist inside its host, macrophages are indispensable to keep *Mtb* infection under control. They recognize invading pathogens at the first stage of infection and initiate the immune response (Medzhitov and Janeway, 2000). Pathogen-associated molecular patterns (PAMPs) and endogenous danger-associated molecular patterns (DAMPs) are recognized by pattern recognition receptors (PRRs), of which the Toll-like receptors (TLR) are one of the major classes (Medzhitov and Janeway, 2000; Matzinger, 2002). Myeloid differentiation factor 88 (MYD88) is a key adaptor protein in the TLR signaling pathway since it is used by all TLRs (except for TLR3) to initiate a pro-inflammatory response (Takeda and Akira, 2004). Its C-terminal TIR domain enables interaction with TLRs or the interleukin-1 receptor (IL1R), and the N-terminal death domain enables the formation of a 'Myddosome' signaling complex, consisting of IL-1 receptor associated kinases (IRAKs). The Myddosome plays a central role in inflammation and host defense by activating the mitogen-activated protein kinase (MAPK) and the nuclear factor- κ B (NF- κ B) signaling pathways (Muzio et al., 1997;

Wesche et al., 1997; Lin et al., 2010; Gay et al., 2011).

Deficiency in MYD88 reduces the ability to induce an appropriate immune response and results in an increased susceptibility to pyogenic bacteria in humans (Netea et al., 2012). MyD88-deficient mice are hyporesponsive to lipopolysaccharide (LPS) and Il-1 stimulation and they are resistant to endotoxic shock (Adachi et al., 1998; Kawai et al., 1999; Akira and Takeda, 2004). In mice, it also resulted in susceptibility to various pathogens, among them *Mtb* (Ryffel et al., 2005).

The zebrafish is naturally susceptible to tuberculosis, caused by a variant of *Mycobacterium marinum* (*Mm*), which is genetically related to *Mtb*, and shows a similar pathogenesis to human disease, including the formation of granulomatous lesions (Swaim et al., 2006, Ramakrishana, 2013). The larval stage of the zebrafish enables detailed *in vivo* imaging and has been used to study host-pathogen interactions during *Mm* infection (Davis et al., 2002). The active recruitment of macrophages during *Mm* infection and the reverse migration of infected macrophages from infected sites, characterizes the dynamic nature of early granulomas (Davis and Ramakrishnan, 2009). In addition to macrophages, also neutrophils have been shown to play an important role during *Mm* infection. Neutrophils recruited to the infection site are able to actively kill the phagocytosed *Mm* by means of oxidative mechanisms (Yang et al., 2012).

In zebrafish larvae, the Myd88-signalling pathway has been shown to have a protective role during *Mm* infection (van der Vaart et al., 2013). Myd88-deficient larvae are shown to have an compromised innate immune response to bacterial infections, affecting the production of pro inflammatory cytokines (van der Vaart et al., 2013; Roca and Ramakrishnan, 2013), production of reactive nitrogen species by neutrophils (Elks et al., 2014) and the initiation of autophagic defence (van der Vaart et al., 2014), resulting in increased rates of infection. In the present study we have used this *myd88* mutant zebrafish line (*myd88*^{-/-}) to study the effect of Myd88 deficiency on granuloma development. To this end we used our previously reported tail fin injection model, where the formation of a single granuloma can be followed over time. Our combined results of light and electron microscopy show that *Mm* infection in *myd88* mutant larvae results in an increased bacterial burden associated with strongly reduced recruitment of leukocytes to granulomas and reduced cell death in the granuloma structures. Furthermore, we have found that in *myd88* mutants the majority of *Mm* was extracellular and that intracellular acidic compartments containing bacteria were less abundant.

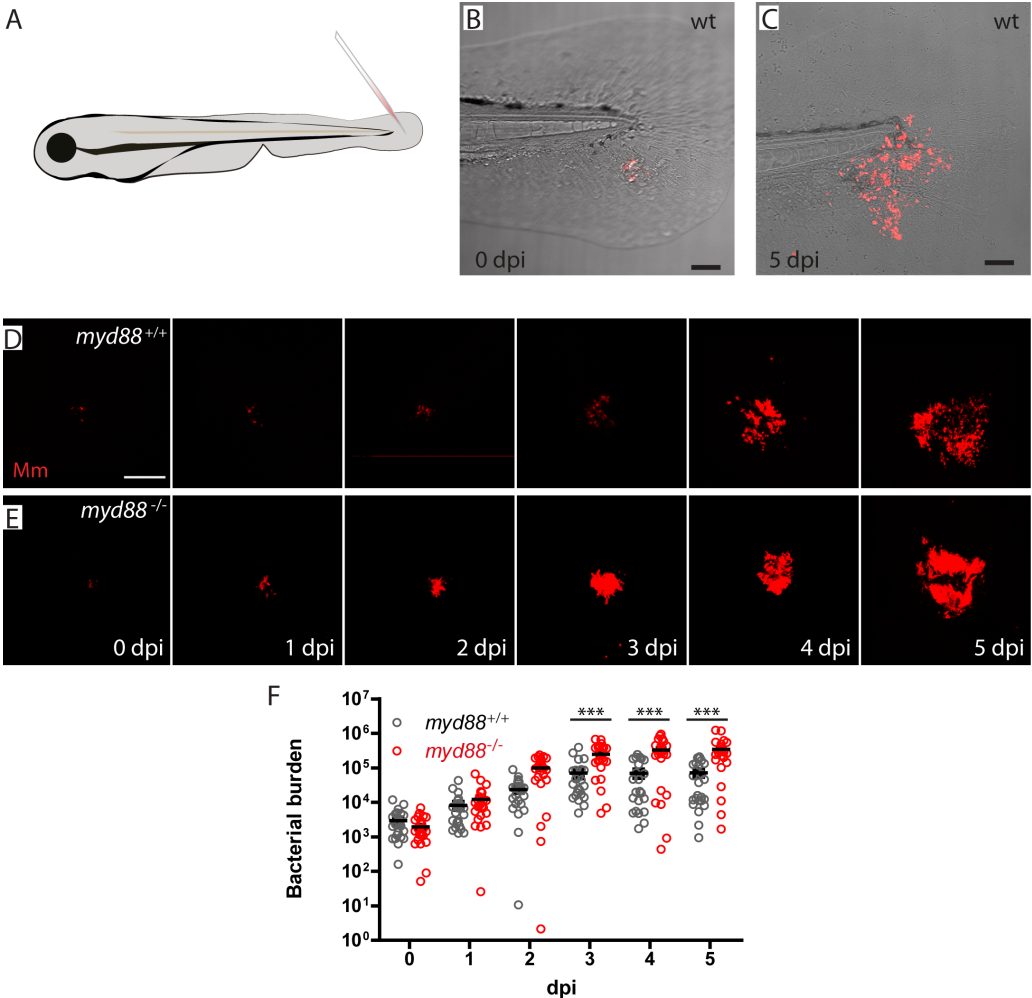


Figure 1. Granuloma development and morphology in the tail fin of zebrafish larvae. **A)** *Mm* injection in the tail fin generates single granuloma. **B and C)** Infected tail fin of the same larva with fluorescently labelled *Mm* (red) at 4 hours post infection (A) and at 4 days post infection (B) showing the localized development of the early granuloma structures. **D and E)** Representative images of larvae showing the increase of *Mm* infection (red) and development of granuloma structures in the wild type (D) and *myd88*^{-/-} larvae (E). **F)** Bacterial burden in the *myd88*^{+/+} (black) and *myd88*^{-/-} (red) larvae. The data (mean ± SEM) were analysed using analysis of variance (ANOVA), Bonferroni's multi comparison post-test was performed on *myd88* wild type and mutant larvae at each timepoint (***, represents $P < 0.0001$, $n > 20$ larvae per time point). The scale bars represent 100 μm .

Results

In order to study the role of TLR/IL1R signalling during *M. marinum* (*Mm*) in zebrafish, larvae were used from a homozygous *myd88* mutant line (*myd88*^{-/-}) (van der Vaart et al., 2013). These larvae were infected with ~50 colony forming units (cfu) of fluorescently labelled *Mm* in the tail fin at 3 dpf. Injection of *Mm* in the tail fin induces a localized infection, which develops into a granuloma-like structure within 3 to 5 days post infection (dpi) (Figure 1A-C; Hosseini et al., 2014).

Granuloma development and bacterial burden

To provide a detailed description of the infection process and the development of the granuloma structure, confocal laser scanning microscopy (CLSM) was performed on the tail fin of infected *myd88*^{-/-} and wild type (*myd88*^{+/+}) larvae. The bacterial burden in representative *myd88*^{+/+} and *myd88*^{-/-} larvae is shown in Figure 1. The infection in each of these larvae was imaged at 4 hours post infection (hpi) and at 1, 2, 3, 4 and 5 days post infection (dpi). From 2dpi onward we observed compacted bacterial aggregates in *myd88*^{-/-} larvae (Figure 1E), while in the *myd88*^{+/+} larvae these aggregates were much smaller and spread over the infected tissue (Figure 1D).

In a separate experiment the bacterial burden was quantified in the *myd88*^{+/+} and *myd88*^{-/-} larvae, based on fixed samples at 0 to 5 dpi (Figure 1F). The bacterial burden was measured as the total volume of the fluorescent signal of *Mm*. The infection size increased significantly between 0 and 3 dpi in the *myd88*^{+/+} and the *myd88*^{-/-} larvae. The infection size increased at a lower rate in the wild type larvae compared to the growth rate in the mutant. At 4dpi the difference in infection size between *myd88*^{+/+} and *myd88*^{-/-} larvae was maximal with $69 \cdot 10^3$ bacteria per μm^3 ($\pm 1.6 \cdot 10^3$) and $328 \cdot 10^3$ bacteria per μm^3 ($\pm 52 \cdot 10^3$), respectively.

Number of leukocytes at the infection site

In order to study the recruitment of leukocytes towards the infection in the tail fin in *myd88*^{-/-} zebrafish, we performed Lcp1/L-plastin immunostaining at 4 dpi for visualization of all leukocytes (Figure 2). The larvae were imaged using CLSM and representative images are shown for *myd88*^{+/+} and *myd88*^{-/-} larvae (Figure 2A and 2B respectively). At 4 dpi the infection in the tail fin has resulted in formation of an initial stage granuloma, which in *myd88*^{+/+} larvae was observed as a large local accumulation of L-plastin positive cells (35.4 ± 4.2) at the site of the infection in the tail fin (Figure 2A and 2C). In the *myd88*^{-/-} larvae the number of L-plastin-positive

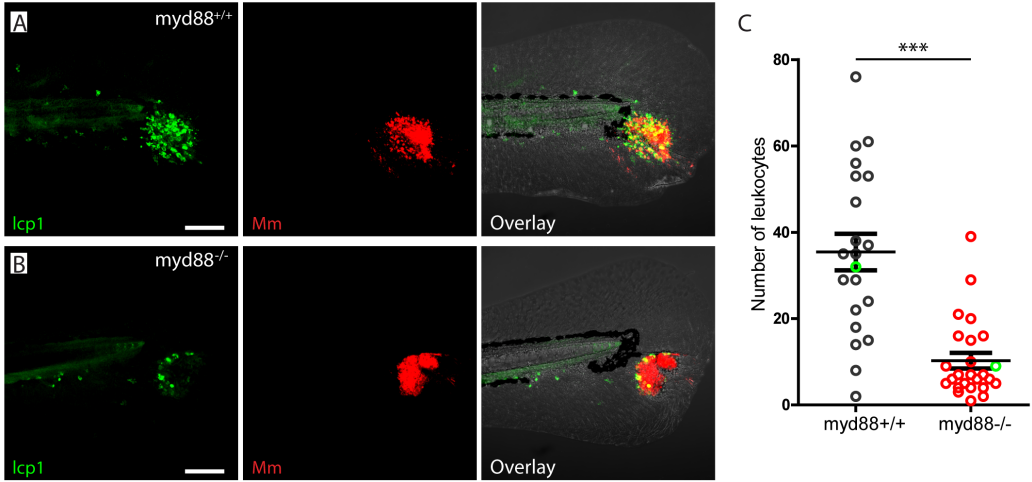


Figure 2. Number of leukocytes at the site of infection in *myd88*^{+/+} and *myd88*^{-/-} larvae. **A and B)** Representative images of a larva showing lcp1-positive cells (green) and *Mm* (red) in *myd88*^{+/+} (A) and *myd88*^{-/-} (B) larvae at 4 dpi. **C)** Quantification of lcp1-positive cell shows less leukocytes to be present at the site of infection in *myd88*^{-/-} larvae. The data (mean ± SEM) were analyzed using a two-tailed student t test (***) indicates $P < 0.001$, $n > 20$ larvae per condition). Scale bar represents 100 μm.

4

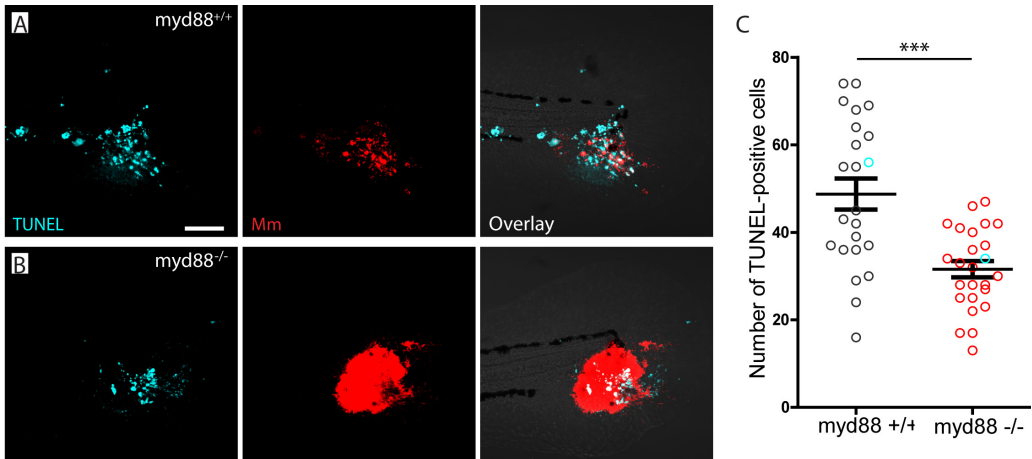


Figure 3. TUNEL-positive cells at the site of infection in *myd88*^{+/+} and *myd88*^{-/-} larvae. **A and B)** Representative images of a larva showing TUNEL-positive cells (green) and *Mm* (red) in *myd88*^{+/+} (A) and *myd88*^{-/-} (B) larvae at 4 dpi. **C)** Quantification of TUNEL-positive cell shows less dead cells to be present at the site of infection in *myd88*^{-/-} larvae. The data (mean ± SEM) were analyzed using a two-tailed student t test (***) indicates $P < 0.001$, $n > 20$ larvae per condition). Scale bar represents 100 μm.

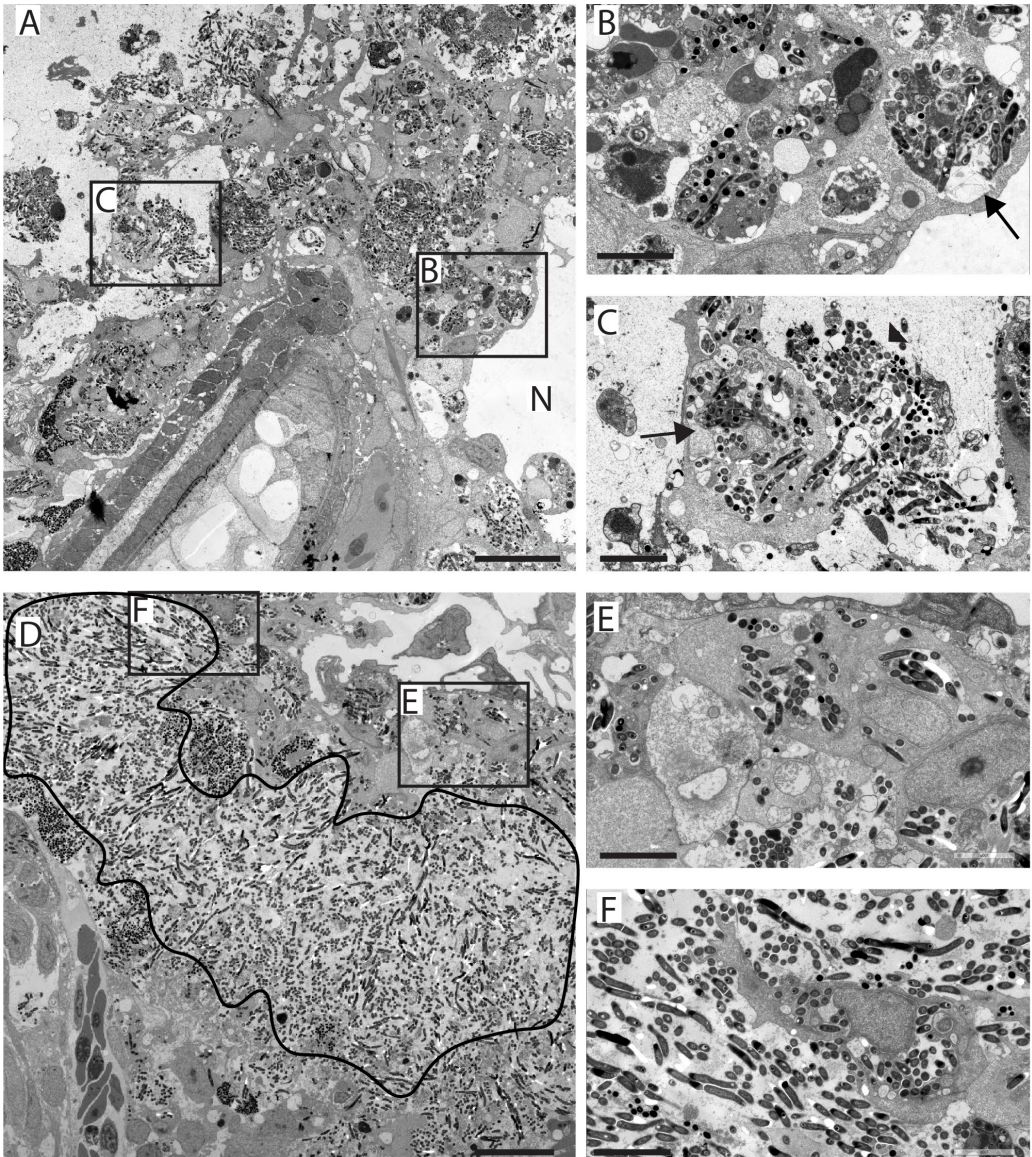


Figure 4. Granuloma structures in *myd88*^{-/-} consist mainly of extracellular *Mm*. **A)** TEM image of a granuloma in representative *myd88*^{+/+} larvae, showing the necrotic centre (N) and aggregates of *Mm* in the immune cells. **B and C)** Higher magnification of regions indicated in **A**, showing infected cells (arrowheads) and extracellular *Mm* (arrows). **D)** TEM image of a granuloma in representative *myd88*^{-/-} larvae showing the area with extracellular *Mm* (black line). **E and F)** Higher magnification of region indicated in **D**, showing extracellular bacteria and infected cells (arrowheads). n=3 per group, the scale bars in A-D; 20 μ m and in B-C and E-F; 10 μ m.

cells at the site of infection was significantly lower (10.2 ± 1.8). The leukocytes in the *myd88*^{-/-} larvae were mainly observed surrounding the site of infection, while in the wild type larvae the leukocytes were observed within the infected area (Figure 2A and 2B).

Number of dead cells at the infection site

The lower number of leukocytes observed at the site of infection in *myd88*^{-/-} larvae could either be due to a lower number of leukocytes recruited to the infected area or to a higher rate of cell death of these cells. To address this issue we performed a fluorescent Terminal deoxynucleotidyl transferase dUTP nick end labelling (TUNEL) assay on *myd88*^{+/+} and *myd88*^{-/-} larvae at 4 dpi, which visualizes double stranded DNA breaks, thereby labelling apoptotic as well as necrotic cells (Figure 3). The *myd88*^{+/+} larvae show a high number of TUNEL positive cells (48.7 ± 3.6) throughout the site of infection (Figure 3A). The *myd88*^{-/-} larvae show a lower number of TUNEL positive cells (31.6 ± 1.8 ; Figure 3B and 3C), which were mainly located at the centre of the infected area. Therefore, it can be concluded that the lower number of leukocytes at infection sites in *myd88*^{-/-} is a consequence of reduced recruitment rather than increased cell death.

Transmission electron microscopy of *Mm* infection in *myd88*^{-/-} larvae

Transmission electron microscopy (TEM) was performed on the tail fin granulomas of *Mm* infected *myd88*^{+/+} larvae and *myd88*^{-/-} larvae, in order to analyze the ultrastructural effects of Myd88 deficiency (Figure 4). At 5dpi, the *myd88*^{+/+} larvae show a necrotic center in the infected area, visible as a hole in the tail fin, which is surrounded by a large number of cells containing bacteria (Figure 4A and 4B). In the *myd88*^{-/-} larvae the majority of bacteria were found to be extracellular (Figure 4C and 4D), and the large area containing these extracellular bacteria was surrounded by infected cells (Figure 4D).

To determine the nature and frequency of different cell-bacterium interactions in *myd88*^{+/+} and *myd88*^{-/-} larvae, we quantified the occurrence of intracellular *Mm* in the cytoplasm without any membrane structures surrounding it, or in different types of intracellular compartments. The analysis of this quantification and representative images of each type of interaction are shown in Figure 5. The majority of intracellular bacteria was found in aggregates (>5 bacteria per compartment), ~64% in *myd88*^{+/+} compared to ~50% in *myd88*^{-/-} larvae (Fig. 5 A and B). However, acidic aggregates, characterized by a lysosomal morphology with uniform electron dense content in the compartment, were less abundant in mutant larvae (~8%) compared to wild type (~39%, Figure 5 B). Individual bacteria were present in phagosomes, characterized by a single membrane with

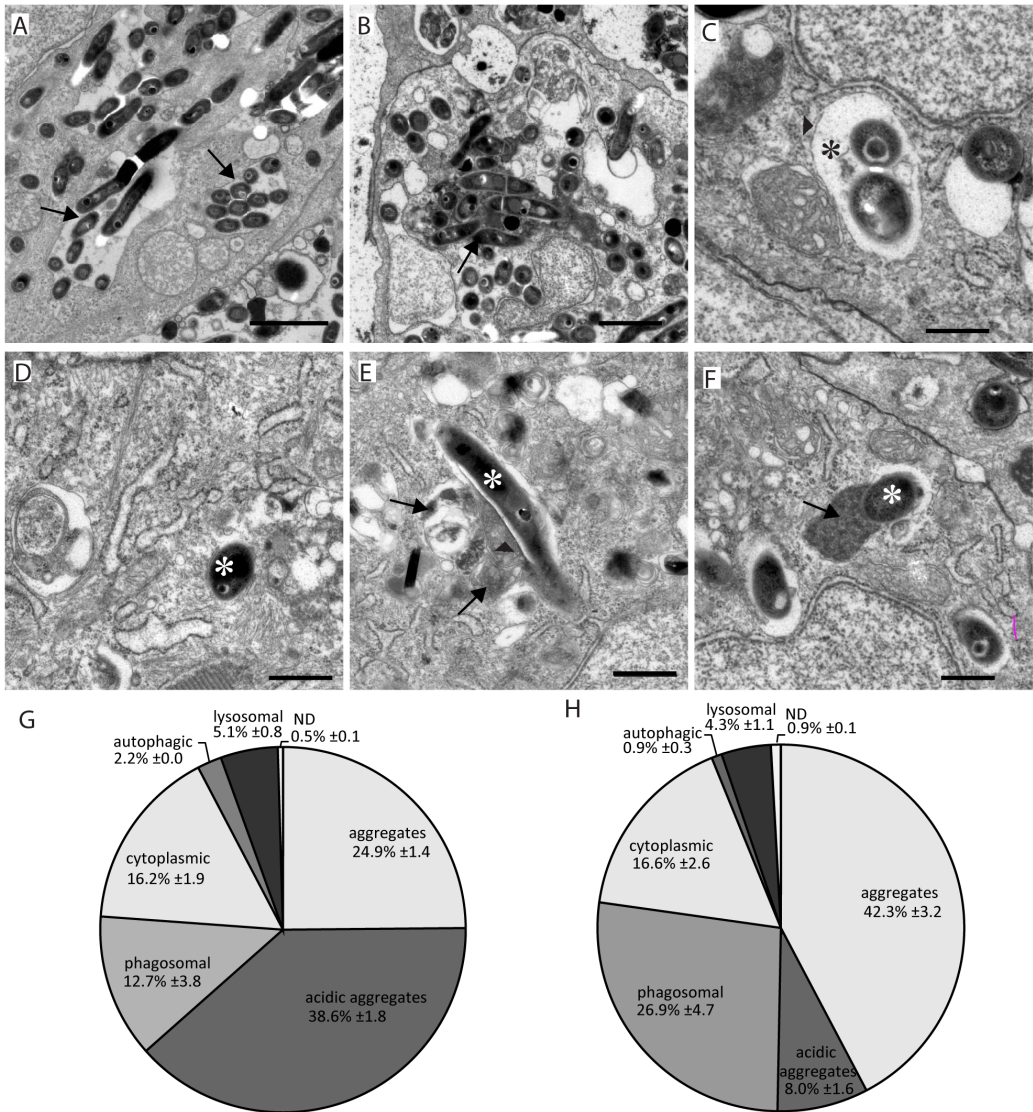


Figure 5. Quantification of intracellular *Mm* shows altered distribution of bacteria in different compartments in *Myd88*^{-/-}. **A to F)** Representative TEM images of *Mm* in different compartments. **A)** Aggregates were observed as a compact cluster of bacteria (<5) without any electron dense areas (arrows). **B)** Acidic aggregates were observed as a compact number of bacteria in a compartment having a uniform electron density between the bacteria (arrowhead) and/or electron dense regions (arrow). **C)** Phagosomal compartment containing bacteria surrounded by a single membrane (arrowhead) with an electron-transparent zone (asterisk), without any cytoplasmic material in the compartment. **D)** Cytoplasmic bacteria are shown not enclosed by any membrane, indicated by a white asterisk. **E)** Autophagic vacuoles containing bacteria (asterisk), with partially degraded content (arrowhead) and other fused vacuoles (arrows). **F)** Lysosomal compartment containing bacteria (asterisk) with

uniform electron dense content (arrow). **G and H**) The fractions (\pm SEM) of intracellular *Mm* found in different compartments or free in the cytoplasm are presented in a pie chart for *myd88*^{+/+} (G) and *myd88*^{-/-} (H). n=3 per group, the scale bars in A-B; 2 μ m and in C-F; 500 nm.

an electron-transparent zone or tightly surrounding the bacteria without any cytoplasmic material (Figure 5C). In mutant larvae \sim 27% of bacteria were found in those phagosomal compartments compared to \sim 13% in the wild types. A similar number of bacteria was found in the cytoplasm, not enclosed by any membrane, in the wild type and mutant larvae (respectively, \sim 16% and \sim 17%, Figure 5D). In addition, bacteria were found in autophagic compartments, in the *myd88*^{+/+} (\sim 2%) and *myd88*^{-/-} (\sim 1%) larvae. These compartments are characterized by partially degraded cytoplasmic content and organelles as a result of engulfment by or fusion with autophagosomes (Figure 5E, Hosseini et al., 2014). Finally, some bacteria were located inside lysosomal compartments (<5 bacteria per compartment) with regular electron dense content in the wild type and *myd88*^{-/-} larvae, at a frequency of respectively \sim 5% and \sim 4% (Figure 5F). In conclusion, the reduced presence of acidic aggregates is the most notable difference between *myd88*^{-/-} and wild type larvae.

Discussion

In this paper we provide new insight in the early stages of granuloma development and structure during *Mm* infection by both light and electron microscopy using the tail fin infection model in zebrafish larvae. We show that localized infection develops in the tail fin of both *myd88*^{+/+} and *myd88*^{-/-} larvae. In the *myd88*^{-/-} larvae the infection developed much faster and showed an increased infection size at 4 dpi. This is consistent with the data shown in a blood island infection model, showing an increased infection size and susceptibility to mycobacterium infection in *myd88*^{-/-} larvae (van der Vaart et al., 2013). In addition, using the tail fin infection model we observed a clear different phenotype of infection in the mutant compared to the wild type larvae (Figure 1D and 1E). The mutant shows more compacted *Mm* in a large aggregated growth spot at the site of infection and electron microscopy showed that the majority of bacteria in this location were extracellular.

The number of leukocytes at the site of infection was significantly lower in the mutant at 4dpi (Figure 2C). This lower number of leukocytes was not due to higher cell death rate of these cells in the mutant larvae, since significantly less TUNEL-positive cells were observed at the site of infection (Figure 3C). This indicated that the low presence of leukocytes is due to reduced recruitment towards the pathogen

in *myd88*^{-/-} larvae. However, the recruitment of leukocytes towards *Mm* infection is not dependent on *myd88* mediated signalling at initial stages of infection (Cambier et al., 2014), as shown in hindbrain infection upon morpholino knock down of *myd88*. Apparently, there is a difference in Myd88 dependency between initial and long-term leukocyte response to *Mm* infection. The long term recruitment is likely to be dependent on the induction of genes for pro-inflammatory mediators including cytokines and leukotrienes and genes encoding tissue remodelling factors like matrix metalloproteinases. These genes are strongly induced along with the expansion of granulomas in zebrafish larvae and the induction of these genes is dependent on *myd88* (van der Vaart et al., 2013). The increased extracellular growth of *Mm* in *myd88*^{-/-} larvae is consisted with results in other systems in which the immune system is compromised, for example knock down of the TNF receptor, (Roach et al., 2002, Tobin et al., 2012). Additionally, we studied the intracellular bacteria that resided in the immune cells of the mutant and the wild type. We already showed that the largest fraction of *Mm* in the wild type larvae were observed in acidic aggregates (Hosseini et al., 2014). Interestingly, a distinct difference was observed in the nature of compartments in which intracellular *Mm* was present. In mutant larvae a much smaller fraction was found in these acidic aggregates and a larger fraction in non-acidic aggregates and phagosomal compartments. It seems that acidification of these larger aggregates is highly Myd88 dependent and helps to restrict bacterial growth, since *myd88* mutants developed severely increased bacterial burden. Alternatively, the differences could be explained by presence of *Mm* in different cell types than leukocytes in the mutant. However, we favour the interpretation that the large acidic bacterial aggregates in the granulomas of wild type larvae result from the efferocytosis of dead infected cells by leukocytes that are recruited to the infection site in a Myd88-dependent manner.

In summary, we have identified a low level of recruitment of leukocytes towards infection at the later stage of *Mm* infection in *myd88* mutants. This is probably due to the decrease in inflammatory responses induced by the *myd88*-NFκB pathway, which results in an increased infection due to uncontrolled mycobacterial growth in non-acidifying compartments of infected cells as well as extracellular growth of bacteria.

Materials and Methods

Zebrafish strains and maintenance

Zebrafish were handled in compliance with the local animal welfare regulations and maintained according to standard protocols (www.zfin.org). The *myd88*^{+/+} and

the *myd88*^{-/-} zebrafish strains were used for this study. All fish were raised and grown at 28.5 °C on a 14 h light : 10 h dark cycle. Embryos were obtained from natural spawning at the beginning of the light period and kept in egg water (60 µg/ml Instant Ocean sea salts).

Zebrafish tail fin infection

The *M. marinum* M strain fluorescently labelled with E2-crimson was used and prepared at ~500 colony-forming units per 1 nl as previously described (Benard et al., 2013). Borosilicate glass microcapillaries (Harvard Apparatus, 300038) were used with a micropipette puller device (Sutter Instruments Inc.) for preparing microinjection needles. Zebrafish larvae were injected in the tail fin at 3 dpf using the Eppendorf microinjection system with a fine (~5 to 10 micron) needle tip broken off with tweezers and mounted at a 30-degree angle. Larvae were anesthetized in egg water with 200 µg/mL 3-aminobenzoic acid (Tricaine; Sigma-Aldrich, E10521) and injected between the 2 epidermal layers at the ventral part of the tail fin (Fig. 1), as previously described (Hosseini et al., 2014). Larvae were fixed at desired time points after infection with 4% paraformaldehyde in PBS-T (phosphate-buffered saline; NaCl 150 mM, K₂HPO₄ 15 mM, KH₂PO₄ 5 mM) with 0.05% Tween 20 (Merck Millipore, 8221840500) with gentle agitation for 18 h at 4 °C. The larvae were washed the next day with PBS-T and stored at 4 °C for further staining or until imaging.

TUNEL assay

The TUNEL experiments were performed using Millipore ApopTag Peroxidase In Situ Apoptosis detection kit and Roche Anti-Digoxigenin-POD Fab fragments using a protocol adapted for use in Zebrafish embryos (Ref). For fluorescent detection Perkin Elmer TSA Fluorescence kits Cy5 and Fluorescein were used.

Confocal laser scanning microscopy

Fixed larvae were mounted in 1% low melting agarose (Sigma-Aldrich, A9414) and imaged with a Leica TCS SPE (Wetzlar, Germany) confocal laser scanning microscope using the 488 and the 633 laser lines with 20X (NA 0.7) and 63X (NA 1.2) objectives. Images were analysed using Fiji software.

Transmission electron microscopy

Before being used for electron microscopy the zebrafish larvae were anesthetized with 200 µg/ml tricaine and afterwards immediately fixated in 2% glutaraldehyde and 2% paraformaldehyde in sodium cacodylate buffer (pH 7.2) for 3 h at room temperature followed by fixation for 16 h at 4 °C. Postfixation was performed in

1% osmium tetroxide in sodium cacodylate buffer for 1 h at room temperature. After dehydration through a graded series of ethanol all specimens were kept in epoxy resin (Agar Scientific, AGR1043) for 16 h before embedding. Ultrathin sections were collected on Formvar coated 200 mesh or one hole copper grids (Agar Scientific, AGS162) stained with 2% uranyl acetate in 50% ethanol and lead citrate for 10 min each. Electron microscopy images were obtained with a JEOL JEM-1010 transmission electron microscope (Tokyo, Japan) equipped with an Olympus Megaview camera (Tokyo, Japan).

Statistical analysis

All data (mean \pm SEM) were analyzed (Prism version 5.0, GraphPad Software) using one-way analysis of variance (ANOVA) with Bonferroni's multi comparison post-test for multiple groups. Two-tailed student t tests was used for comparing 2 conditions.

References

- Adachi, O., T. Kawai, K. Takeda, M. Matsumoto, H. Tsutsui, M. Sakagami, K. Nakanishi, and S. Akira. 1998. Targeted disruption of the MyD88 gene results in loss of IL-1- and IL-18-mediated function. *Immunity*. 9:143–150.
- Akira, S., and K. Takeda. 2004. Toll-like receptor signalling. *Nat Rev Immunol*. 4:499–511. doi:10.1038/nri1391.
- Alonso, S., K. Pethe, D.G. Russell, and G.E. Purdy. 2007. Lysosomal killing of Mycobacterium mediated by ubiquitin-derived peptides is enhanced by autophagy. *Proc. Natl. Acad. Sci. U.S.A.* 104:6031–6036. doi:10.1073/pnas.0700036104.
- Armstrong, J.A., and P.D. Hart. 1971. Response of cultured macrophages to Mycobacterium tuberculosis, with observations on fusion of lysosomes with phagosomes. *J. Exp. Med.* 134:713–740. doi:10.1084/jem.134.3.713.
- Benard, E.L., A.M. van der Sar, F. Ellett, G.J. Lieschke, H.P. Spaink, and A.H. Meijer. 2012. Infection of zebrafish embryos with intracellular bacterial pathogens. *J Vis Exp*. doi:10.3791/3781.
- Bortoluci, K.R., and R. Medzhitov. 2010. Control of infection by pyroptosis and autophagy: role of TLR and NLR. *Cell. Mol. Life Sci*. 67:1643–1651. doi:10.1007/s00018-010-0335-5.
- Cambier, C.J., K.K. Takaki, R.P. Larson, R.E. Hernandez, D.M. Tobin, K.B. Urdahl, C.L. Cosma, and L. Ramakrishnan. 2014. Mycobacteria manipulate macrophage recruitment through coordinated use of membrane lipids. *Nature*. 505:218–222. doi:10.1038/nature12799.

- Davis, J.M., and L. Ramakrishnan. 2009. The role of the granuloma in expansion and dissemination of early tuberculous infection. *Cell*. 136:37–49. doi:10.1016/j.cell.2008.11.014.
- Davis, J.M., H. Clay, J.L. Lewis, N. Ghori, P. Herbomel, and L. Ramakrishnan. 2002. Real-time visualization of mycobacterium-macrophage interactions leading to initiation of granuloma formation in zebrafish embryos. *Immunity*. 17:693–702.
- Deng, Q., E.A. Harvie, and A. Huttenlocher. 2012. Distinct signalling mechanisms mediate neutrophil attraction to bacterial infection and tissue injury. *Cellular Microbiology*. 14:517–528. doi:10.1111/j.1462-5822.2011.01738.x.
- Elks, P.M., M. van der Vaart, V. van Hensbergen, E. Schutz, M.J. Redd, E. Murayama, H.P. Spaink, and A.H. Meijer. 2014. Mycobacteria counteract a TLR-mediated nitrosative defense mechanism in a zebrafish infection model. *PLoS ONE*. 9:e100928. doi:10.1371/journal.pone.0100928.
- Gay, N.J., M. Gangloff, and L.A.J. O'Neill. 2011. What the Myddosome structure tells us about the initiation of innate immunity. *Trends in Immunology*. 32:104–109. doi:10.1016/j.it.2010.12.005.
- Gengenbacher, M., and S.H.E. Kaufmann. 2012. Mycobacterium tuberculosis: success through dormancy. *FEMS Microbiology Reviews*. 36:514–532. doi:10.1111/j.1574-6976.2012.00331.x.
- Goldberg, D.E., R.F. Siliciano, and W.R. Jacobs. 2012. Outwitting evolution: fighting drug-resistant TB, malaria, and HIV. *Cell*. 148:1271–1283. doi:10.1016/j.cell.2012.02.021.
- Hosseini, R., G.E. Lamers, Z. Hodzic, A.H. Meijer, M.J. Schaaf, and H.P. Spaink. 2014. Correlative light and electron microscopy imaging of autophagy in a zebrafish infection model. *autophagy*. 10:1844–1857. doi:10.4161/auto.29992.
- Kawai, T., O. Adachi, T. Ogawa, K. Takeda, and S. Akira. 1999. Unresponsiveness of MyD88-deficient mice to endotoxin. *Immunity*. 11:115–122.
- Koul, A., E. Arnoult, N. Lounis, J. Guillemont, and K. Andries. 2011. The challenge of new drug discovery for tuberculosis. *Nature*. 469:483–490. doi:10.1038/nature09657.
- Lin, P.L., C.B. Ford, M.T. Coleman, A.J. Myers, R. Gawande, T. Ioerger, J. Sacchettini, S.M. Fortune, and J.L. Flynn. 2014. Sterilization of granulomas is common in active and latent tuberculosis despite within-host variability in bacterial killing. *Nat. Med.* 20:75–79. doi:10.1038/nm.3412.
- Lin, S.-C., Y.-C. Lo, and H. Wu. 2010. Helical assembly in the MyD88-IRAK4-IRAK2 complex in TLR/IL-1R signalling. *Nature*. 465:885–890. doi:10.1038/nature09121.
- Matzinger, P. 2002. The danger model: a renewed sense of self. *Science*. 296:301–305. doi:10.1126/science.1071059.
- Medzhitov, R., and C. Janeway. 2000. The Toll receptor family and microbial recognition. *Trends Microbiol.* 8:452–456.
- Muzio, M., J. Ni, P. Feng, and V.M. Dixit. 1997. IRAK (Pelle) family member IRAK-2 and MyD88 as proximal mediators of IL-1 signaling. *Science*. 278:1612–1615.
- Netea, M.G., C. Wijmenga, and L.A.J. O'Neill. 2012. Genetic variation in Toll-like receptors and disease susceptibility. *Nat. Immunol.* 13:535–542. doi:10.1038/ni.2284.

- Ramakrishnan, L. 2013. Looking within the zebrafish to understand the tuberculous granuloma. *Adv. Exp. Med. Biol.* 783:251–266. doi:10.1007/978-1-4614-6111-1_13.
- Roach, S.K., and J.S. Schorey. 2002. Differential regulation of the mitogen-activated protein kinases by pathogenic and nonpathogenic mycobacteria. *Infect. Immun.* 70:3040–3052.
- Roach, S.K., S.-B. Lee, and J.S. Schorey. 2005. Differential activation of the transcription factor cyclic AMP response element binding protein (CREB) in macrophages following infection with pathogenic and nonpathogenic mycobacteria and role for CREB in tumor necrosis factor alpha production. *Infect. Immun.* 73:514–522. doi:10.1128/IAI.73.1.514-522.2005.
- Roca, F.J., and L. Ramakrishnan. 2013. TNF dually mediates resistance and susceptibility to mycobacteria via mitochondrial reactive oxygen species. *Cell.* 153:521–534. doi:10.1016/j.cell.2013.03.022.
- Russell, D.G. 2007. Who puts the tubercle in tuberculosis? *Nat. Rev. Microbiol.* 5:39–47. doi:10.1038/nrmicro1538.
- Russell, D.G., C.E. Barry, and J.L. Flynn. 2010. Tuberculosis: what we don't know can, and does, hurt us. *Science.* 328:852–856. doi:10.1126/science.1184784.
- Ryffel, B., C. Fremont, M. Jacobs, S. Parida, T. Botha, B. Schnyder, and V. Quesniaux. 2005. Innate immunity to mycobacterial infection in mice: critical role for toll-like receptors. *Tuberculosis.* 85:395–405. doi:10.1016/j.tube.2005.08.021.
- Sasindran, S.J., and J.B. Torrelles. 2011. Mycobacterium Tuberculosis Infection and Inflammation: what is Beneficial for the Host and for the Bacterium? *Front. Microbio.* 2:2. doi:10.3389/fmicb.2011.00002.
- Simeone, R., F. Sayes, O. Song, M.I. Gröschel, P. Brodin, R. Brosch, and L. Majlessi. 2015. Cytosolic access of Mycobacterium tuberculosis: critical impact of phagosomal acidification control and demonstration of occurrence in vivo. *PLoS Pathog.* 11:e1004650. doi:10.1371/journal.ppat.1004650.
- Swaim, L.E., L.E. Connolly, H.E. Volkman, O. Humbert, D.E. Born, and L. Ramakrishnan. 2006. Mycobacterium marinum infection of adult zebrafish causes caseating granulomatous tuberculosis and is moderated by adaptive immunity. *Infect. Immun.* 74:6108–6117. doi:10.1128/IAI.00887-06.
- Takeda, K., and S. Akira. 2004. Microbial recognition by Toll-like receptors. *J. Dermatol. Sci.* 34:73–82. doi:10.1016/j.jdermsci.2003.10.002.
- Tobin, D.M., F.J. Roca, S.F. Oh, R. McFarland, T.W. Vickery, J.P. Ray, D.C. Ko, Y. Zou, N.D. Bang, T.T.H. Chau, J.C. Vary, T.R. Hawn, S.J. Dunstan, J.J. Farrar, G.E. Thwaites, M.-C. King, C.N. Serhan, and L. Ramakrishnan. 2012. Host genotype-specific therapies can optimize the inflammatory response to mycobacterial infections. *Cell.* 148:434–446. doi:10.1016/j.cell.2011.12.023.
- van der Vaart, M., C.J. Korbee, G.E.M. Lamers, A.C. Tengeler, R. Hosseini, M.C. Haks, T.H.M. Ottenhoff, H.P. Spaink, and A.H. Meijer. 2014. The DNA damage-regulated autophagy modulator DRAM1 links mycobacterial recognition via TLP-MYD88 to autophagic defense. *Cell Host and Microbe.* 15:753–767. doi:10.1016/j.chom.2014.05.005.
- van der Vaart, M., J.J. van Soest, H.P. Spaink, and A.H. Meijer. 2013. Functional analysis of a zebrafish myd88 mutant identifies key transcriptional components of the innate immune system. *Dis Model Mech.* 6:841–854. doi:10.1242/dmm.010843.

- van der Wel, N., D. Hava, D. Houben, D. Fluitsma, M. van Zon, J. Pierson, M. Brenner, and P.J. Peters. 2007. M. tuberculosis and M. leprae Translocate from the Phagolysosome to the Cytosol in Myeloid Cells. *Cell*. 129:1287–1298. doi:10.1016/j.cell.2007.05.059.
- Vergne, I., R.A. Fratti, P.J. Hill, J. Chua, J. Belisle, and V. Deretic. 2004. Mycobacterium tuberculosis phagosome maturation arrest: mycobacterial phosphatidylinositol analog phosphatidylinositol mannoside stimulates early endosomal fusion. *Molecular Biology of the Cell*. 15:751–760. doi:10.1091/mbc.E03-05-0307.
- Wesche, H., C. Korherr, M. Kracht, W. Falk, K. Resch, and M.U. Martin. 1997. The interleukin-1 receptor accessory protein (IL-1RAcP) is essential for IL-1-induced activation of interleukin-1 receptor-associated kinase (IRAK) and stress-activated protein kinases (SAP kinases). *J. Biol. Chem.* 272:7727–7731.
- Yang, C.-T., C.J. Cambier, J.M. Davis, C.J. Hall, P.S. Crosier, and L. Ramakrishnan. 2012. Neutrophils exert protection in the early tuberculous granuloma by oxidative killing of mycobacteria phagocytosed from infected macrophages. *Cell Host and Microbe*. 12:301–312. doi:10.1016/j.chom.2012.07.009.
- Zhang, J., S. Liu, K.V. Rajendran, L. Sun, Y. Zhang, F. Sun, H. Kucuktas, H. Liu, and Z. Liu. 2013. Pathogen recognition receptors in channel catfish: III phylogeny and expression analysis of Toll-like receptors. *Developmental & Comparative Immunology*. 40:185–194. doi:10.1016/j.dci.2013.01.009.

